Available online at www.sciencedirect.com
ScienceDirect
Journal of Sound and Vibration 304 (2007) 230–245
JOURNAL OF SOUND AND VIBRATION
www.elsevier.com/locate/jsvi

Active vibration control of smart grid structure by multiinput and multioutput positive position feedback controller

Moon K. Kwak*, Seok Heo

Department of Mechanical Engineering, Dongguk University, 26 Pil-Dong 3-Ga, Joong-Gu, Seoul 100-715, Republic of Korea

Received 7 November 2006; accepted 23 February 2007
Available online 16 April 2007

Abstract

This paper is concerned with the active vibration control of a grid structure equipped with piezoceramic sensors and actuators. The grid structure is a replica of the solar panel commonly mounted on satellites, which contains complex natural mode shapes. The multiinput and multioutput positive position feedback (PPF) controller is considered as an active vibration controller for the grid structure. A new concept, the block-inverse technique, is proposed to cope with more modes than the number of actuators and sensors. This study also deals with the stability and the spillover effect associated with the application of the multiinput multioutput PPF controller based on the block-inverse technique. It was found that the theories developed in this study are capable of predicting the control system characteristics and its performance. The new multiinput multioutput PPF controller was applied to the test structure using a digital signal processor and its efficacy was verified by experiments.

1. Introduction

A smart structure is defined as one that contains distributed sensors, actuators and a control scheme to achieve vibration suppression in close cooperation. Conceptually, the smart structure should be able to cope with external disturbances and internal changes. There are many materials that have been tested for actuators and sensors. They are piezoelectric materials, shape memory alloys, electrostrictive materials, magnetostrictive materials, electro-theological fluids, and fiber optics. These materials can be inserted into or bonded with structures thus acting as sensor or actuator. Among them, piezoelectric materials have become popular because of high strength, temperature insensitivity, and ease of implementation. If a voltage is applied to the piezoelectric material, then it undergoes deformations. On the contrary, a charge is produced when deformation occurs. Hence, it can be used both sensor and actuator.

The most popular piezoelectric material is the piezoceramic material consisting of lead zirconate titanite. In particular, the piezoceramic plate can be easily glued to the surface of structures. The analysis on the smart structure equipped with piezoelectric sensors and actuators was initially performed on the beam structures. Crawley et al. [1,2] discussed the modeling technique applicable to the beam structure with bonded

*Corresponding author. Tel.: +82 2 2260 3705; fax: +82 2 2263 9379.
E-mail address: kwakm@dongguk.edu (M.K. Kwak).

0022-460X/$ - see front matter © 2007 Elsevier Ltd. All rights reserved.
doi:10.1016/j.jsv.2007.02.021

piezoceramic sensors and actuators. Hanagud et al. [3] used the finite element method to model the smart structure and suppressed the vibration with rate-modal feedback and optimal control. Fanson and Caughy [4] proposed the use of the positive position feedback (PPF) controller based on the modal displacement signal. Poh and Baz [5] improved the PPF controller for the multidegree-of-freedom system using the independent modal space control concept [6]. The relationship between the PPF controller and the output feedback controller was investigated by Friswell and Inman [7]. The stability condition, the performance, and the design methodology was studied by Kwak et al. [8]. Many researchers extended the smart structure theory to different types of structures [9–11].

The PPF controller is very effective in suppressing a specific vibration mode, thus maximizing the damping in a targeted frequency bandwidth without destabilizing other modes [7]. The transfer function of the single-input and single-output (SISO) PPF controller is equal to the one of a simple low-pass filter circuit, allowing it to be easily realized by either an operational amplifier or a microprocessor [12]. For this reason, the PPF controller has been widely used as the active vibration controller for smart structures. However, the natural vibration characteristics should be known a priori either theoretically or experimentally in order to successfully apply the PPF controller, which is sometimes called the tuning process.

This paper is concerned with active vibration suppression of a grid structure equipped with piezoceramic sensors and actuators. The grid structure shown in Fig. 1 is similar to a solar panel mounted on satellites. The vibration of the solar panel must be controlled to maintain the attitude and pointing accuracy as well as to protect electronic devices sensitive to vibrations. The grid structure built for the demonstration of the active vibration control technique consists of two piezoceramic sensors and two pairs of piezoceramic actuators, which are glued to the surface of the composite grid structure. This study deals with the dynamic modeling of the grid structure equipped with piezoceramic sensors and actuators.

The test setup results in a two-input and two-output control system, which is a typical multiinput and multioutput (MIMO) system. Hence, this problem poses the vibration control issue of the grid structure,

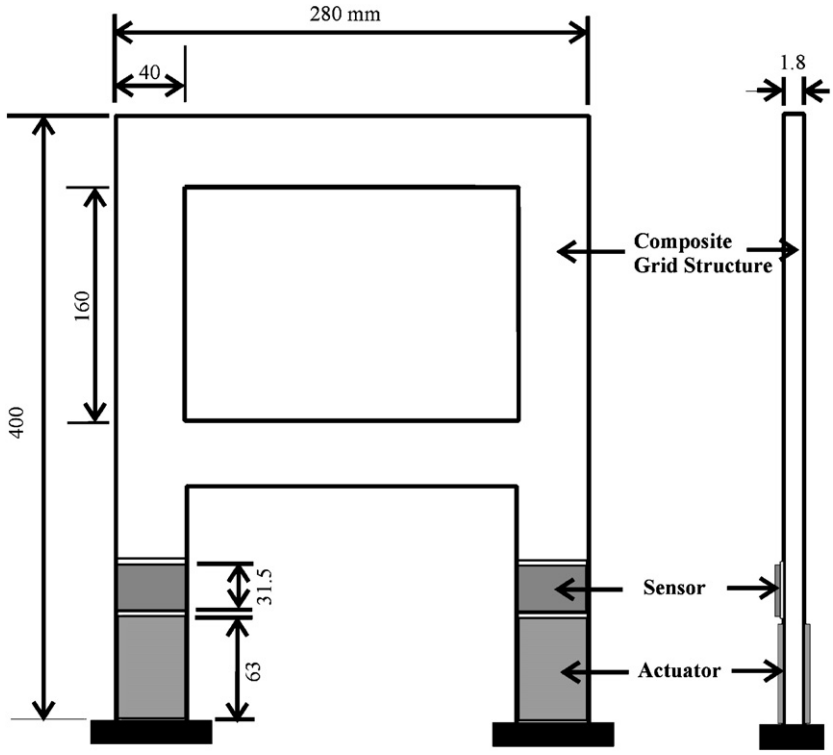

Fig. 1. Smart grid structure.

which has infinite number of complex modes with a finite number of sensors and actuators. If the number of sensors and actuators are smaller than the number of modes to be controlled, then the actual control force can be reconstructed from the modal control forces using the pseudo-inverse technique. However, it was found both theoretically and experimentally that the control authority on each mode is lost during the pseudo-inverse process. A new reconstruction scheme based on the block-inverse technique which is capable of producing more reasonable control forces from the modal control forces is developed in this study.

The block-inverse technique employed in implementing the MIMO PPF controller inherently leads to the control and measurement spillover problem as other control techniques do [7,8], which are related directly to the stability. In this study, the stability and spillover problems associated with the MIMO PPF controller are discussed in detail. It is found that the theories developed in this study are capable of predicting the control system characteristics and its performance. The MIMO PPF controller was then applied to the test structure using a digital signal processor. It is found from experiments that the new MIMO PPF controller based on the block-inverse technique can suppress the lowest four modes of the grid structure with two sensors and two actuators without spillover to higher modes.

2. Theoretical modeling of smart grid structure

A smart composite grid structure that is considered in this research is shown in Fig. 1. The composite grid structure was designed and manufactured using carbon/epoxy fabric prepreg (Hankook Carbon Co. CF-3327) and glass/epoxy fabric prepreg (Hankook Fiber Co. G635). During the lay-up procedure, 4 plies of carbon/epoxy were stacked and insulated by a ply of glass/epoxy layer on top and bottom surfaces. The stacked plate was cured in autoclave and cut as shown in Fig. 1.

Copper foil wires were placed on both surfaces for electrodes. Piezoceramic wafers were then bonded on the surface of glass/epoxy outer layer using 90-min cure epoxy. Silver epoxy (Daejoo Precision Co. DS-7276-A) was then used as bond between electrode of ceramic and copper foil wire. Large piezoceramic plates (63.5 mm L × 38.1 mm W) were used as actuators and small piezoceramic plates (25.4 mm L × 38.1 mm W) were used as sensors. In order to induce a larger moment to suppress the vibration of main structure, each piezoceramic actuator is bonded on both sides of the structure, which acts adversely thus doubling the actuator force. Table 1 shows material properties and we used PZT-5A from Morgan Matroc Inc. as actuator and sensor.

The resulting grid structure is the system equipped with two sensors and two actuators as shown in Fig. 1, in which actuators are bonded in the root of the grid structure and small sensors are bonded close to the actuators to make a nearly collocated system. The grid structure, which is in fact a continuous system, has an infinite number of natural frequencies and modes. As can be seen from Fig. 1, the structure is actually a three-dimensional structure. However, we assume Euler–Bernoulli-type laminate theory, which neglects shear deformation for the structure, so that it can be modeled by the grid finite element with two angular displacements and a transverse displacement if lower modes are of prime interest for control. To this end, the equivalent bending stiffness was estimated based on the composite beam theory. The total number of nodal points and elements are 24, respectively. Each nodal point has three degrees of freedom and the two nodal points are fixed, thus resulting 66 degrees of freedom model. Fig. 2 shows the finite element model used for this

Table 1
Material properties of PZT-5A

Property	Value
Piezoelectric charge (d_{31})	-171×10^{-12} m/V
Thickness	0.25 mm
Elastic modulus (E)	61 GPa
Density (ρ)	7700 kg/m^3
Poisson's ratio (υ)	0.3

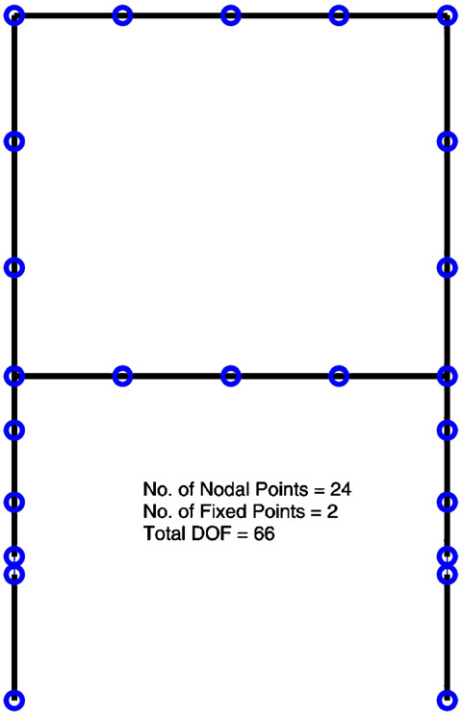

Fig. 2. The finite element modeling.

study, where o indicates the nodal point. The followings are element mass and stiffness matrices used in the finite element formulation.

$$m_e = \begin{bmatrix} 2b & 0 & 0 & b & 0 & 0 \\ 0 & 156g & 22Ig & 0 & 54g & -13Ig \\ 0 & 22Ig & 4I^2g & 0 & 13Ig & -3I^2g \\ b & 0 & 0 & 2b & 0 & 0 \\ 0 & 54g & 13Ig & 0 & 156g & -22Ig \\ 0 & -13Ig & -3I^2g & 0 & -22Ig & 4I^2g \end{bmatrix}, \tag{1}$$

$$k_e = \begin{bmatrix} d & 0 & 0 & -d & 0 & 0 \\ 0 & 12a & 6La & 0 & -12a & 6La \\ 0 & 6La & 4L^2a & 0 & -6La & 2L^2a \\ -d & 0 & 0 & d & 0 & 0 \\ 0 & -12a & -6La & 0 & 12a & -6La \\ 0 & 6La & 2L^2a & 0 & -6La & 4L^2a \end{bmatrix}, \tag{2}$$

where $b = \bar{J}L/6$ and $g = \bar{m}I/420$, $a = \mathrm{EI}/L^3$, $d = \mathrm{GJ}/L$ in which $\bar{J}$ is the polar mass moment of inertia per unit length, L is the element length, $\bar{m}$ is the mass per unit length, I is the sectional area moment of inertia, EI is the bending stiffness, and GJ is the torsional stiffness, respectively.

The actuation moment resulting from two piezoceramic wafers bonded to the both sides of the grid structure can be approximated by the couple acting on its ends [15]. Based on this assumption, each moment

can be written as

$$M_p = E_p w_p t_b d_{31} v_a, \tag{3}$$

where E_p is the Young's modulus of the piezoceramic wafer, w_p the width of the piezoceramic actuator, t_b the thickness of the grid structure, d_{31} the piezoelectric constant, and v_a the actuator voltage, respectively. The piezoceramic wafer can be also used as a sensor. In this case, the charge induced by the deformation turns into the sensor voltage after the signal is processed by a charge amplifier [15], which can be approximately expressed as follows:

$$v_s = -\frac{E_p w_p t_b d_{31}}{2C_c}(\alpha_2 - \alpha_1), \tag{4}$$

where C_c is the capacitance of the piezoceramic sensor and α_1, α_2 are the slope of the grid at both ends of the piezoceramic sensor, respectively.

Considering Eqs. (1)–(4), the resulting equations of motion for the smart grid structure shown in Fig. 1 can be written as

$$M\ddot{x} + C\dot{x} + Kx = B_a v_a, \quad v_s = C_s x, \tag{5a,b}$$

where x is an $m \times 1$ nodal displacement vector, M, C, K are $m \times m$ mass, damping, and stiffness matrices, m is the total degrees of freedom for the finite element model, B_a is an $m \times \ell$ actuator participation matrix, C_s is an $\ell \times m$ sensor participation matrix, ℓ is the number of actuators and sensors, respectively. In our case, ℓ is equal to 2. Eq. (5a) represents the structure equation associated with the actuator forces and Eq. (5b) represents the sensor equation, respectively.

Natural frequencies and natural mode shapes can then be obtained by solving the eigenvalue problem. First four mode shapes are plotted in Fig. 3. As can be seen from Fig. 3, the grid structure contains bending modes, which are symmetric about the middle line and torsional modes, which are axisymmetric about the middle line. In fact, the first and the third natural modes are the bending modes similar to the bending modes of the beam and the second and the fourth natural modes are the torsional modes. The theoretical and experimental natural frequencies are tabulated in Table 2. The experimental natural frequencies were obtained by FFT signal analyzer. Fig. 4 shows experimental setup to obtain the transfer function between the actuator and sensor. As shown in the figure, the random noise generated by the dynamic signal analyzer is added to the control voltage by the adder circuit consisting of an operational amplifier. The sensor signal was then fed to the dynamic signal analyzer and the A/D port of the controller board. In this way, we can measure the frequency response function and control the system simultaneously.

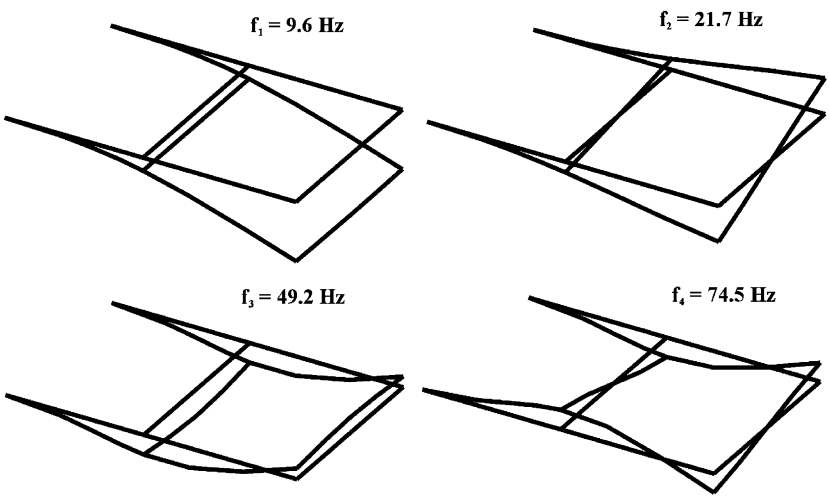

Fig. 3. Natural frequencies and modes of the grid structure.

Table 2
Theoretical and experimental natural frequencies (unit: Hz)

Mode	Theory	Experiment
1	9.60	9.63
2	21.72	20.00
3	49.23	47.63
4	74.50	68.13
5	98.82	104.75
6	146.42	140.75

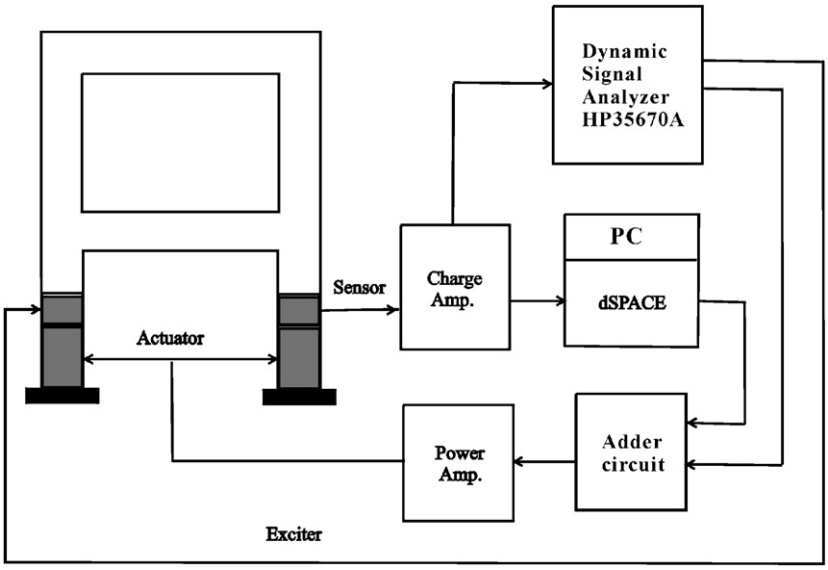

Fig. 4. Experimental setup.

We can reduce the equations of motion given by Eq. (5) by introducing the reduced-order modal coordinates:

$$x = Uq, \tag{6}$$

where q is an $n \times 1$ generalized displacement vector and U is an $m \times n$ eigenvector matrix which in fact represent the lower modes of interest. Using the orthogonality property of the eigenvalues and eigenvectors, $U^{\mathrm{T}}MU = I$, $U^{\mathrm{T}}KU = \Lambda = \Omega^2$, and assuming $U^{\mathrm{T}}CU = 2Z\Omega$, we can transform Eq. (5) into the reduced-order modal equations:

$$\ddot{q} + 2Z\Omega\dot{q} + \Lambda q = \bar{B}_a v_a, \quad v_s = \bar{C}_s q, \tag{7a,b}$$

where I is an $n \times n$ identity matrix, Ω is an $n \times n$ eigenvalue matrix, and Z is an $n \times n$ damping factor matrix, $\bar{B}_a = U^{\mathrm{T}}B_a$, $\bar{C}_s = C_s U$, respectively, in which $\bar{B}_a$ is an $n \times \ell$ actuator participation matrix and $\bar{C}_s$ is an $\ell \times n$ sensor participation matrix based on the modal coordinates.

The input–output relation of Eq. (7) is in fact the transfer function between the sensor and actuator and can be derived by using Laplace transform. The theoretical and experimental frequency response plots of the transfer function are shown in Fig. 5. As shown in Fig. 5, there exists a good agreement between the theoretical predictions and experimental results up to the sixth mode. The damping factor of 0.005 is assumed for the all modes in the theoretical model.

We do not need all the modes for the control design, so that we considered only four modes. Hence, we will design the MIMO PPF controller based on the four natural modes of interest. The numerical data for the

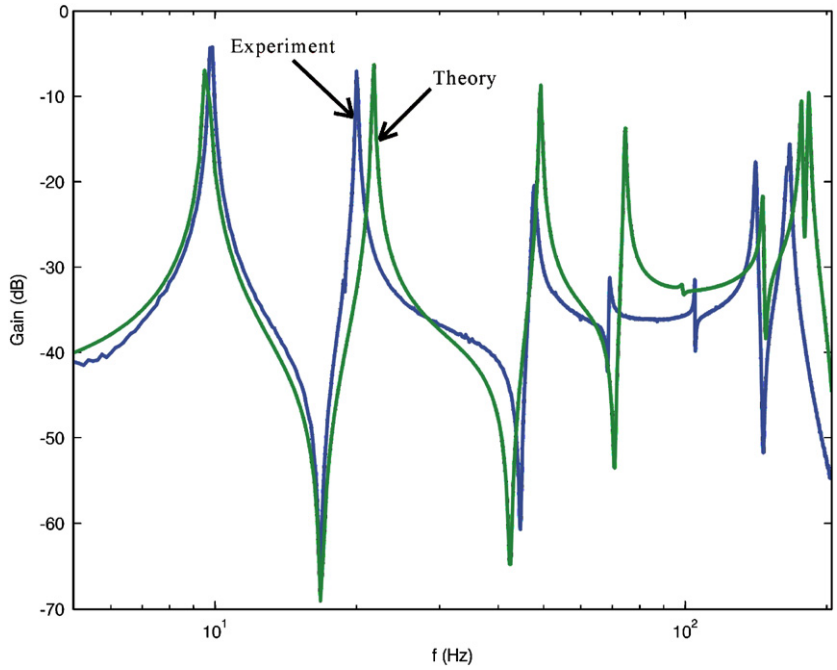

Fig. 5. Theoretical and experimental frequency response plots.

matrices shown in Eq. (7) are as follows:

$$\Lambda = \mathrm{diag}(3637.1,\ 18625.8,\ 95662.8,\ 219085.6),$$

$$2Z\Omega = \mathrm{diag}(0.603,\ 1.365,\ 3.903,\ 4.681),$$

$$\bar{B}_a = \begin{bmatrix} -0.0033 & -0.0033 \\ 0.0063 & -0.0063 \\ -0.0175 & -0.0175 \\ -0.0250 & 0.0250 \end{bmatrix},$$

$$\bar{C}_s = \begin{bmatrix} -10693 & -15733 & -20881 & -18038 \\ -10693 & 15733 & -20881 & 18038 \end{bmatrix}.$$

3. Single-input and single-output PPF control

Before designing the MIMO PPF controller for the addressed problem, it is worthwhile to study the single-input single-output (SISO) PPF controller. The SISO PPF controller was initially proposed by Fanson and Caughy [4] and it has been used successfully for the active vibration control of smart structures using piezoceramic sensor and actuator. The SISO PPF controller was developed to cope with the single-degree-of-freedom vibration system, where the equations consists of two equations, one describing the structure and one describing the compensator [4]:

$$\ddot{\xi} + 2\varsigma\omega\dot{\xi} + \omega^2\xi = g\omega^2\eta, \quad \ddot{\eta} + 2\varsigma_f\omega_f\dot{\eta} + \omega_f^2\eta = \omega_f^2\xi, \tag{8a,b}$$

where g is the scalar gain >0, ξ the modal displacement for the structure, η the compensator coordinate, ω, ω_f the structural and compensator frequencies, respectively, and ς, ς_f the structural and compensator damping ratios, respectively. As can be seen in Eq. (8), the compensator equation is the same as the structural modal

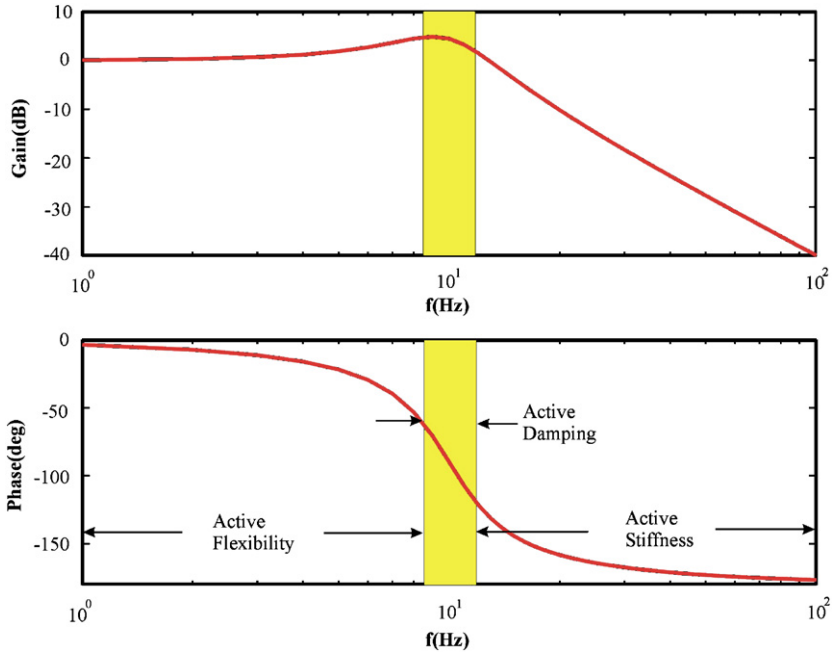

Fig. 6. Bode diagram for the SISO PPF controller.

equation but with higher damping ratio. The PPF terminology stems from the fact that the compensator coordinate is positively fed back into Eq. (8a). For the coupled structure–control problem given by Eq. (8), the absolute stability is guaranteed for $g<1$ [4,8]. The active damping of the closed-loop system depends on the PPF filter frequency, the gain and the damping factor of the PPF controller. The formula was derived in Ref. [8] for the active damping ratio when the PPF filter frequency is tuned to the structural natural frequency:

$$\varsigma_c = \varsigma + \frac{g}{4\varsigma_f}, \tag{9}$$

where ς_c is the resultant damping ratio by the SISO PPF controller. If $g = 0.1$, $\varsigma_f = 0.3$, the active damping factor of 8.3% can be added to the target natural frequency.

The transfer function of the PPF compensator given by Eq. (8b) can be expressed in terms of Laplace variable:

$$H(s) = \frac{\omega_f^2}{s^2 + 2\varsigma_f\omega_f s + \omega_f^2}, \tag{10}$$

which is in fact a second-order low-pass filter, so that we can utilize an equivalent analog circuit easily [12]. Fig. 6 shows the frequency response plot of the PPF compensator. It can be readily understood from Fig. 6 that the cut-off frequency of the PPF compensator has -90° phase shift with slightly higher magnitude. This is why the PPF control can act as an active damping for the specific frequency and needs fine-tuning. The magnitude of the frequency response plot indicates that the SISO PPF controller has less spillover to higher frequency modes as the magnitude rolls off above the cut-off frequency [7]. However, the SISO PPF controller may lead to spillover problem to lower frequency modes when the feedback gain is high.

4. Multiinput and multioutput PPF control

As implied by Eq. (7a), the control force is to be calculated based on the modal space. In this case, the MIMO modal PPF controller can be written as

$$\ddot{Q} + 2Z_f\Omega_f\dot{Q} + \Lambda_f Q = G^{1/2}\Lambda_f\hat{q}, \tag{11}$$

where Q is an $n \times 1$ coordinate vector of the modal PPF controller, Z_f is an $n \times n$ damping factor matrix of the MIMO PPF controller, Ω_f is an $n \times n$ compensator frequency matrix, $\Lambda_f = \Omega_f^2$, and G is an $n \times n$ gain matrix, respectively. Q represents the modal control force vector and each modal control force is to be computed by the SISO PPF compensator based on the corresponding modal displacement. Eq. (11) is decoupled but the actual control force, v_a is to be computed from modal control forces. $\hat{q}$ is the estimation of modal displacement and introduced because they are to be computed based on the sensor measurement. Hence, the control system is internally decoupled but externally coupled. Even though the structural equations of motion given by Eq. (7a) is a reduced-order system, there are still two problems involved in applying the MIMO PPF controller to the real system. The first problem is the computation of the actuation voltage using the modal control forces. The second problem is the estimation of the modal displacement based on the sensor measurements.

Let us discuss the first problem. In order for structural equation of motion, Eq. (7a) to be compatible with the MIMO PPF controller, Eq. (11), the following relation should hold.

$$\bar{B}_a v_a = G^{1/2} \Lambda Q. \tag{12}$$

If $n = \ell$, i.e., the number of actuators is equal to the number of modes to be controlled, then $\bar{B}_a$ becomes a square matrix. If $\bar{B}_a$ is non-singular, then the actuator voltage, v_a can be obtained from the modal control force vector, Q by inverting $\bar{B}_a$. However, if $n > \ell$, i.e., there are more modes to be controlled than the number of available actuators, we come across the over-determined case. This amounts to the case that we try to control many modes with a limited number of actuators. We can think of the pseudo-inverse technique to estimate the actuation voltages from the modal PPF control forces as follows:

$$v_a = (\bar{B}_a)^{\dagger} G^{1/2} \Lambda Q, \tag{13}$$

where $(\bar{B}_a)^{\dagger} = (\bar{B}_a^{\mathrm{T}} \bar{B}_a)^{-1} \bar{B}_a^{\mathrm{T}}$ represents the pseudo inverse. Even though the control force estimated by the above formula can successfully suppress vibrations of four natural modes with two actuators and two sensors, it has been observed that the pseudo-inverse technique results in uneven distribution of control authority on each mode. As a result, the control performance can not be predicted accurately. Let us discuss this problem further by inserting Eq. (13) into Eq. (7a):

$$\ddot{q} + 2Z\Omega\dot{q} + \Lambda q = \bar{B}_a (\bar{B}_a)^{\dagger} G^{1/2} \Lambda Q. \tag{14}$$

In order for Eq. (13) to be a pair with the MIMO PPF controller given by Eq. (11), the resultant of matrix multiplication $\bar{B}_a(\bar{B}_a)^{\dagger}$ should be at least close to identity matrix. However, for the numerical data obtained for the smart grid structure, we obtained

$$\bar{B}_a(\bar{B}_a)^{\dagger} = \begin{bmatrix} 0.035 & 0 & 0.183 & 0 \\ 0 & 0.059 & 0 & -0.236 \\ 0.183 & 0 & 0.905 & 0 \\ 0 & -0.236 & 0 & 0.941 \end{bmatrix}. \tag{15}$$

It becomes evident from Eq. (15) that the diagonals of the matrix are not unity. Hence, the pseudo-inverse technique used for the estimation of actuation voltage does not result in the expected control authority as the SISO PPF controller does.

To avoid the control authority problem, we propose a new approach based on a block-inverse technique, which is applicable to the case of $n = 2\ell, n = 4\ell, \ldots$, i.e., the number of controlled modes is even number times the number of available actuators and each block matrix is non-singular. We resort our case to $n = 2\ell$ in order to simplify the implementation. To this end, let us decompose the actuator participation matrix into two sub matrices as follows:

$$\bar{B}_a = \begin{bmatrix} \bar{B}_{a1} \\ \bar{B}_{a2} \end{bmatrix}. \tag{16}$$

Each sub matrix is an $\ell \times \ell$ square matrix and assumed to be non-singular. Let us then express the actuator voltage as follows:

$$v_a = B_a^* G^{1/2} \Lambda Q, \tag{17}$$

where a new matrix consists of inverse of each sub matrix

$$B_a^* = \left[\left(\bar{B}_{a1}\right)^{-1} \quad \left(\bar{B}_{a2}\right)^{-1} \right]. \tag{18}$$

Hence, the equations of motion for this case can be rewritten as

$$\ddot{q} + 2Z\Omega\dot{q} + \Lambda q = \hat{B} G^{1/2} \Lambda Q, \tag{19}$$

where

$$\hat{B} = \bar{B}_a B_a^* = \begin{bmatrix} I & \bar{B}_{a1}\left(\bar{B}_{a2}\right)^{-1} \\ \bar{B}_{a2}\left(\bar{B}_{a1}\right)^{-1} & I \end{bmatrix} = \begin{bmatrix} I & \widehat{B}_{12} \\ \widehat{B}_{21} & I \end{bmatrix}. \tag{20}$$

For the numerical data of the smart grid structure, we obtained

$$\hat{B} = \begin{bmatrix} 1 & 0 & 0.190 & 0 \\ 0 & 1 & 0 & -0.250 \\ 5.277 & 0 & 1 & 0 \\ 0 & -3.995 & 0 & 1 \end{bmatrix}. \tag{21}$$

Let us compare Eq. (21) with Eq. (15). It can be readily seen that the matrix of Eq. (21) holds the unity diagonals. This is a very desirable property from the control point of view. The off-diagonal elements of the matrices shown in Eqs. (15) and (21) represent the control spillover effects. Remembering the fact that the PPF controller has control spillover to lower modes, the upper off-diagonal elements should be smaller than the diagonal elements. The lower off-diagonal elements do not play a major role in the MIMO PPF control because the PPF controller has no spillover problem to higher modes as stated earlier. In view of this fact, the matrix of Eq. (21) is more desirable than the one of Eq. (15).

The second problem is the observer spillover problem as stated earlier. The number of sensor is always not enough to measure all the modal coordinates. The MIMO PPF controller equation given by Eq. (11) is valid only if true modal displacements are either obtainable or measurable. In reality, we can only estimate the modal displacements based on the sensor measurements. Our problem amounts to the case of estimating more modal displacements with less sensor measurements, which can be said mathematically the under-determined case. The pseudo-inverse technique can also be applied to estimate the modal displacements based on Eq. (7b) as follows:

$$\hat{q} = (\bar{C}_s)^{\dagger} v_s, \tag{22}$$

where $(\bar{C}_s)^{\dagger} = \bar{C}_s^{\mathrm{T}}(\bar{C}_s\bar{C}_s^{\mathrm{T}})^{-1}$ represents the pseudo-inverse. Inserting Eq. (7b) into (22), we obtain

$$\hat{q} = (\bar{C}_s)^{\dagger}\bar{C}_s q. \tag{23}$$

It can be easily understood that the product of matrix multiplication $(\bar{C}_s)^{\dagger}\bar{C}_s$ should be a unity matrix to make a one-to-one matching. However, the pseudo-inversion formula causes the same unbalanced matrix problem as in the estimation of actuator voltage from the modal PPF control forces. In this study, we propose the block-inverse technique used for the estimation of modal displacements from the sensor measurements. We used the same assumption that the number of modes to be controlled is twice the number of sensors. Let us first decompose the sensor participation matrix into two sub-matrices:

$$\bar{C}_s = \left[\bar{C}_{s1} \quad \bar{C}_{s2} \right]. \tag{24}$$

Then, the estimate of modal coordinates can be written as

$$\hat{q} = C_s^* v_s, \tag{25}$$

where

$$C_s^* = \begin{bmatrix} (\bar{C}_{s1})^{-1} \\ (\bar{C}_{s2})^{-1} \end{bmatrix}. \tag{26}$$

Inserting Eq. (7b) into Eq. (25), we can obtain

$$\hat{q} = \hat{C}q, \tag{27}$$

where

$$\hat{C} = C_s^* \bar{C}_s = \begin{bmatrix} I & (\bar{C}_{s1})^{-1}\bar{C}_{s2} \\ (\bar{C}_{s2})^{-1}\bar{C}_{s1} & I \end{bmatrix}. \tag{28}$$

As can be seen from Eq. (28), the matrix multiplication results in the unity diagonals on the contrary to the pseudo-inverse formula, which is a desirable property from the measurement point of view. If we use the numerical data, we obtain

$$(\bar{C}_s)^{\dagger}\bar{C}_s = \begin{bmatrix} 0.208 & 0 & 0.406 & 0 \\ 0 & 0.432 & 0 & -0.495 \\ 0.406 & 0 & 0.792 & 0 \\ 0 & -0.495 & 0 & 0.568 \end{bmatrix}, \tag{29}$$

$$\hat{C} = \begin{bmatrix} 1 & 0 & 1.953 & 0 \\ 0 & 1 & 0 & -1.146 \\ 0.512 & 0 & 1 & 0 \\ 0 & -0.872 & 0 & 1 \end{bmatrix}. \tag{30}$$

On the contrary to the computation of actuator voltage, the upper off-diagonal elements of the matrix do not degrade the performance of the PPF controller since the PPF controller is in fact a low-pass filter. However, the lower off-diagonal elements should be smaller than the diagonal elements because the lower mode components of the measurement signal can be fed into the PPF controller designed for the higher mode. In view of this fact, it can be readily understood that the new methodology of implementing the MIMO PPF controller proposed in this paper is more effective than the pseudo-inverse technique.

5. Stability of MIMO PPFC

Inserting Eq. (27) into Eq. (11), the MIMO PPFC compensator equation can be rewritten as

$$\ddot{Q} + 2Z_f\Omega_f\dot{Q} + \Lambda_f Q = G^{1/2}\Lambda_f\hat{C}q. \tag{31}$$

By combining Eqs. (7a), (17) and (31), we can write the coupled structure-compensator equation in matrix form

$$\begin{Bmatrix} \ddot{q} \\ \ddot{Q} \end{Bmatrix} + \begin{bmatrix} 2Z\Omega & 0 \\ 0 & 2Z_f\Omega_f \end{bmatrix} \begin{Bmatrix} \dot{q} \\ \dot{Q} \end{Bmatrix} + \begin{bmatrix} \Lambda & -\hat{B}G^{1/2}\Lambda \\ -G^{1/2}\Lambda_f\hat{C} & \Lambda_f \end{bmatrix} \begin{Bmatrix} q \\ Q \end{Bmatrix} = \begin{Bmatrix} 0 \\ 0 \end{Bmatrix}. \tag{32}$$

In order for the coupled equation (32) to be stable, the following condition should be satisfied [4]:

$$\begin{bmatrix} \Lambda & -\widehat{B}\,G^{1/2}\Lambda \\ -G^{1/2}\Lambda_f\,\widehat{C} & \Lambda_f \end{bmatrix} > 0. \tag{33}$$

If $\ell = n$, $\Lambda_f = \Lambda$, and the control is collocated, then the system is absolutely stable when $G < I$ [4]. But in our case, we can only say that the system is stable only when the gain matrix is sufficiently small [8]. For the

addressed problem, we tested the stability with $\Lambda_f = \Lambda$ and $G = gI$ and the instability occurs when $g > 0.2$. Therefore, the stability is guaranteed for sufficiently small G.

6. Control spillover problem of MIMO PPF controller

As stated above, the PPF control needs fine-tuning to be effective in vibration control. However, the control spillover occurs when applying the MIMO PPF controller and furthermore it causes the frequency shift in lower frequency modes when the higher modes are to be controlled by the PPF controller. If we consider the frequency response plot shown in Fig. 6, we can see that the SISO PPF controller can result in added flexibility to the frequency region lower than the cut-off frequency and added stiffness to the frequency region higher than the cut-off frequency. However, the added stiffness to the higher frequency region does not pose any problem as the magnitude rolls off in that region. But the added flexibility may cause problem because of unity gain. This phenomenon was observed in the experiments when a highly amplified actuation signal is fed to the piezoceramic actuator. This problem is known to be a static instability but was never explained theoretically in detail. This problem is also directly related to the choice of the filter frequency matrix, Λ_f.

Let us write rth modal equation from Eq. (19):

$$\ddot{q}_r + 2\varsigma_r\omega_r\dot{q}_r + \omega_r^2 q_r = \sum_{j=1}^{n} \hat{b}_{rj} g_j^{1/2} \omega_j^2 Q_j$$

$$= \sum_{j=1}^{r-1} \hat{b}_{rj} g_j^{1/2} \omega_j^2 Q_j + \hat{b}_{rr} g_r^{1/2} \omega_r^2 Q_r + \sum_{j=r+1}^{n} \hat{b}_{rj} g_j^{1/2} \omega_j^2 Q_j. \tag{34}$$

In deriving Eq. (34), we assume that $G = \mathrm{diag}[g_1 \ g_2, \ldots, g_n]$ and $\widehat{b_{ij}}$ is the element of $\hat{B}$. Due to the frequency characteristics of the SISO PPF controller as shown in Fig. 6, we can assume the following:

$$Q_j = \begin{cases} 0, & j < r. \\ g_j^{1/2} \hat{c}_{jr} q_r, & j > r, \end{cases} \tag{35}$$

where $\hat{c}_{jr}$is the element of $\hat{C}$. Hence, Eq. (34) can be rewritten as

$$\ddot{q}_r + 2\varsigma_r\omega_r\dot{q}_r + \left(\omega_r^2 - \sum_{j=r+1}^{n} \hat{b}_{rj} g_j^{1/2} \omega_j^2 \hat{c}_{jr}\right) q_r = \hat{b}_{rr} g_r^{1/2} \omega_r^2 Q_r. \tag{36}$$

It can be readily seen that the PPF controller tuned to the specific natural mode causes the frequency shift to the lower frequency modes. The frequency shift phenomena imply that the tuning of the MIMO PPF controller should be carried out from the highest mode in descending order. In our study, the 1st and 3rd modes are the bending modes and the 2nd and 4th modes are the torsional modes. The bending modes and torsional modes are decoupled to each other as indicated by $\hat{B}$ and $\hat{C}$ matrices. Hence, the PPF control of the 3rd bending mode only affects the 1st bending mode and the PPF control of the 4th torsional mode only affect the 2nd torsional mode. In order to verify the shift formula given by Eq. (36), we used the gains, $g_3 = 0.0549$, $g_4 = 0.0362$ for the 3rd and 4th modes, respectively and let the 1st and 2nd modes uncontrolled. The approximate shifts for the 1st and 2nd natural modes calculated by using Eq. (36) were found to be 0.7 and 1.0 Hz, respectively, which are confirmed by the frequency response plot shown in Fig. 7. However, the shift in lower natural frequency due to the higher-mode control by PPF controller can not be a great concern because the PPF controller is very robust in vicinity of the target frequency. However, in this study, the tuning of the PPF controller on each mode is to be made to the newly shifted natural frequencies for the full implementation of the MIMO PPF controller, after calculating the frequency shifts of the 1st and 2nd modes.

It should be noted here that the effective control bandwidth of the PPF controller depends on the damping factor of the PPF controller. If a small number is used for the damping factor, then we can get higher active damping as shown in Eq. (9) but it needs more precise tuning. If a large number is used for the damping factor, then the gain should be increased to get more active damping but the control bandwidth is widened. The damping factor of 0.3 has been generally accepted for the real implementation.

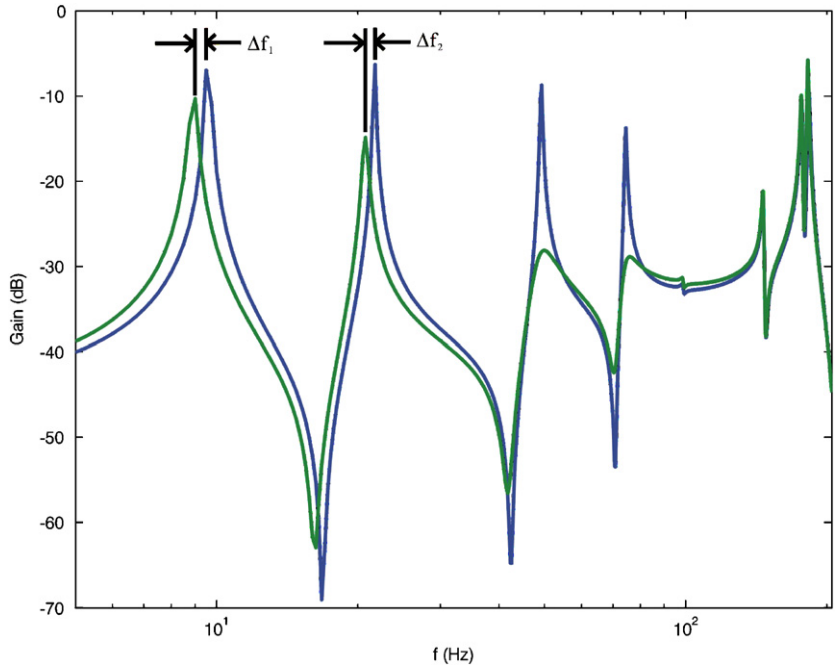

Fig. 7. The frequency shifts due to control spillover.

7. Implementation of MIMO PPF controller

The inputs to the MIMO PPF controller are the piezoelectric sensor measurement voltages and the outputs of the MIMO PPF controller are the actuation voltages to the piezoceramic actuators. Hence, we need the input–output transfer function of the MIMO PPF controller to be practically implemented. Using Eqs. (13), (11) and (25), the following equation for the MIMO PPF controller can be obtained in the form of transfer function

$$V_a(s) = B_a^* G^{1/2} \Lambda H_{\text{ppf}}(s) G^{1/2} C_s^* V_s(s), \tag{37}$$

where

$$H_{\text{ppf}}(s) = \begin{bmatrix} H_1(s) & 0 & 0 & 0 \\ 0 & H_2(s) & 0 & 0 \\ 0 & 0 & H_3(s) & 0 \\ 0 & 0 & 0 & H_4(s) \end{bmatrix}, \tag{38}$$

$$H_i(s) = \frac{\omega_{fi}^2}{s^2 + 2\varsigma_f \omega_{fi} s + \omega_{fi}^2}, \quad i = 1, 2, 3, 4. \tag{39}$$

We chose the damping factor, $\varsigma_f = 0.3$ and the gain matrix, $G = \text{diag}(0.1,\ 0.045,\ 0.018,\ 0.012)$. The filter frequency of each PPF controller is tuned to the natural frequency of target mode. The frequency shift caused by the gain turned out to be small, so that it was neglected in the implementation. The uncontrolled and controlled frequency response plots based on the theoretical model are shown in Fig. 8. It can be seen from Fig. 8 that lower four modes are controlled successfully.

The MIMO PPF controller given by Eq. (37) was realized by the dSpace DSP board, DS1102 [13] along with Simulink [14]. The Simulink block diagram that amounts to Eq. (37) is shown in Fig. 9, which was downloaded to the DSP board. The sampling rate for the A/D and D/A was set to 50 kHz, which is fast

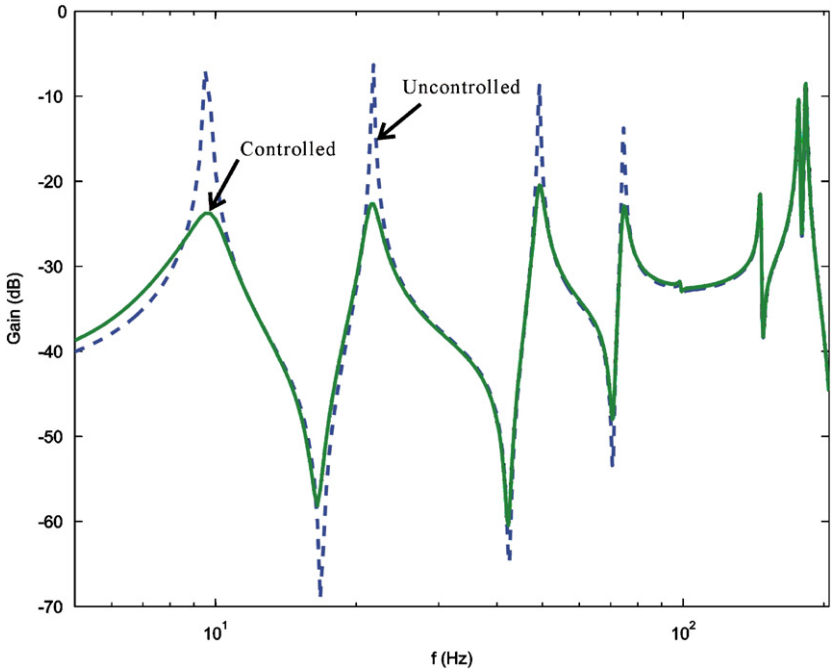

Fig. 8. Uncontrolled and controlled frequency response plots based on the theoretical model.

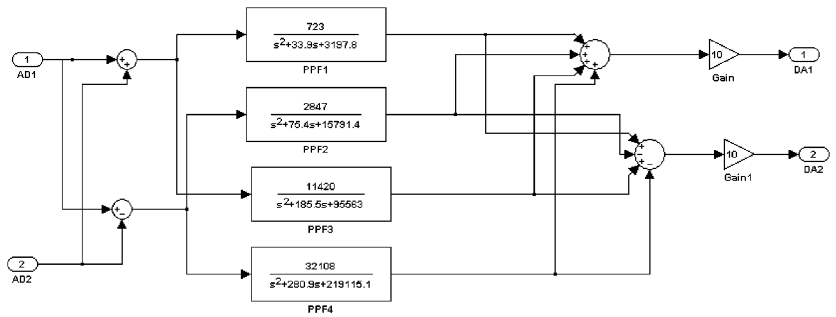

Fig. 9. SIMULINK block diagram for the MIMO PPF controller.

enough to control four modes of interest. Fig. 10 shows the uncontrolled and controlled frequency response plots obtained by experiments. It can be confirmed by experiment that the control performance is close to the one expected theoretically, which validates the proposed control methodology. Fig. 11 shows the uncontrolled and controlled time responses of the sensor output. After the grid structure was excited, the MIMO PPF controller was activated at $t = 1$ s. It can be concluded from the experiment that the proposed MIMO PPF controller is capable of suppressing vibrations of the grid structure successfully.

8. Summary and conclusions

A new MIMO PPF controller based on the block-inverse technique is proposed to suppress many modes of structure with the limited number of actuators and sensors. The composite grid structure equipped with two piezoceramic sensors and two piezoceramic actuators was considered as a test article. Our mission objective is to control as many modes as possible. To this end, the theoretical model for the composite grid structure was derived using the grid finite element method and compared to the experimental result, which shows a good

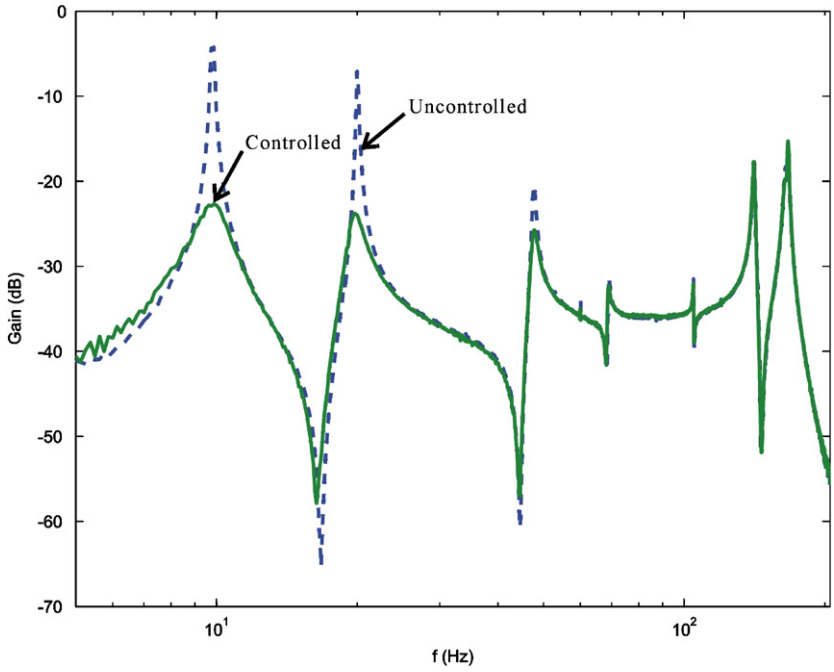

Fig. 10. Uncontrolled and controlled frequency response plots from experiments.

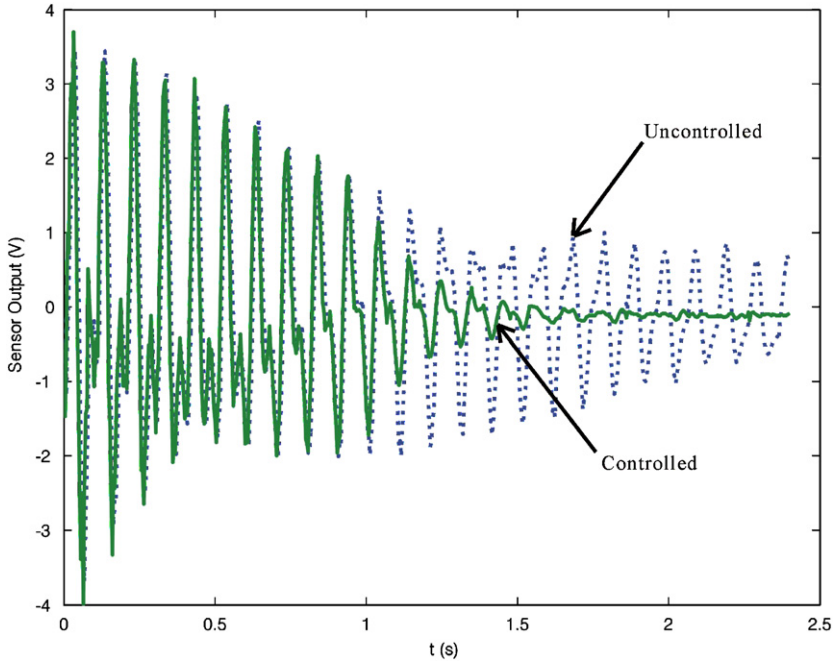

Fig. 11. Uncontrolled and controlled time responses of sensor output.

agreement. The resulting equations of motion were then transformed into the reduced modal equations of motion for control.

Even though it is better to have the same number of actuators and sensors as the number of modes to be controlled, it is not practical. The pseudo-inverse technique can be used to cope with the problem of tackling more modes with the limited number of actuators and sensors. But it results in the poor control authority on

each mode. Hence, we proposed in this study the block-inverse technique, which can preserve the control authority evenly distributed on each mode.

Both the pseudo- and block-inverse techniques have spillover problems, which may destabilize the system. This study shows that the stability MIMO PPF controller is guaranteed if the gain is small. The spillover affect the closed-loop system characteristics thus resulting in the frequency shifts. The approximate formula, which can accurately predict the frequency shift was derived in this study. It was concluded that the tuning of the MIMO PPF controller should be carried out in descending order from the highest mode considering the frequency shifts.

The implementation of the MIMO PPF controller was discussed in detail both theoretically and experimentally. The MIMO PPF controller designed in this study was applied to the test structure using a digital signal processor. Both theoretical and experimental results show that the proposed MIMO PPF controller is capable of suppressing first four modes of the grid structure with two sets of sensor and actuator. It can be concluded that the block inverse technique, the stability prediction formula, and the design methodology can be effectively used for the design of successful vibration suppression controller for smart structures.

Acknowledgments

This research was supported by the Dongguk University Research Fund.

References

[1] E.F. Crawley, J. de Luis, Use of piezoelectric actuators as elements of intelligent structures, *AIAA Journal* 25 (10) (1987) 1373–1385.
[2] E.F. Crawley, E.H. Anderson, Detailed models of piezoceramic actuation of beams, *Journal of Intelligent Material Systems and Structures* 1 (1) (1990) 4–25.
[3] S. Hanagud, M.W. Obal, A.J. Calise, Optimal vibration control by the use of piezoceramic sensors and actuators, *Journal of Guidance, Control, and Dynamics* 15 (5) (1992) 1199–1206.
[4] J.L. Fanson, T.K. Caughey, Positive position feedback control for large space structures. *Proceedings of the 28th structural dynamics conference*, Monterey, CA, 1987, pp. 588–598.
[5] S. Poh, A. Baz, Active control of a flexible structure using a modal positive position feedback controller, *Journal of Intelligent Material Systems and Structures* 1 (3) (1990) 273–288.
[6] L. Meirovitch, H. Baruh, Control of self-adjoint distributed-parameter systems, *Journal of Guidance, Control and Dynamics* 5 (3) (1982) 60–66.
[7] M.I. Friswell, D.J. Inman, The relationship between positive position feedback and output feedback controllers, *Smart Materials and Structures* 8 (3) (1999) 285–291.
[8] M.K. Kwak, S.-B. Han, S. Heo, The stability conditions, performance and design methodology for the positive position feedback controller, *Journal of the Korean Society of Noise and Vibration Engineers* 14 (3) (2004) 208–213 (in Korean).
[9] K.K. Denoyer, M.K. Kwak, Dynamic modelling and vibration suppression of a slewing active structure utilizing piezoelectric sensors and actuators, *Journal of Sound and Vibration* 189 (1) (1996) 13–31.
[10] M.K. Kwak, D. Sciulli, Fuzzy-logic based vibration suppression of a slewing active structure utilizing piezoceramic sensors and actuators, *Journal of Sound and Vibration* 191 (1) (1996) 15–28.
[11] W.-S. Hwang, H.C. Park, W. Hwang, Vibration control of a laminated plate with piezoelectric sensor/actuator: finite element formulation and modal analysis, *Journal of Intelligent Material Systems and Structures* 4 (3) (1993) 317–329.
[12] S. Heo, K.-Y. Kim, M.K. Kwak, Implementation of PPF controller using analog circuit and microprocessor, *Journal of the Korean Society of Noise and Vibration Engineers* 14 (6) (2004) 455–462 (in Korean).
[13] ⟨http://www.dspaceinc.com⟩.
[14] ⟨http://www.mathworks.com⟩.
[15] B.N. Agrawal, H.C. Bang, Active vibration control of flexible space structures by using piezoelectric sensors and actuators, *ASME, Vibration and Control of Mechanical Systems* DE-61 (1993) 169–179.